*Journal of Marine Research, 46,* 753–770, 1988

# The late summer vertical nutrient mixing in Long Island Sound

by Dake Chen,[1] Sarah G. Horrigan[1] and Dong-Ping Wang[1]

ABSTRACT

The occurrence of vertical nutrient mixing in central Long Island Sound was simulated for the period from July 23 to August 29, 1986 using a one-dimensional mixed-layer model based on Mellor and Yamada (1974)'s level 2 turbulence closure scheme.

During most of the study period, the water column was stratified and the nutrient fluxes through the thermocline were driven by the combined effect of the wind and the tidal mixing. The nutrient entrainment at the bottom of the thermocline was tidally induced, while that at the top of the thermocline had a pulsating character resulting from the interaction of the wind stress and wind-generated inertial currents. Near the end of the summer, the combination of strong wind stress, surface cooling and spring tide completely broke down the stratification. The relieved upward nutrient transport was an order of magnitude larger than during the stratified period, which could result in the observed phytoplankton bloom.

Model results agreed well with observations, suggesting that the mixed-layer model can be used for prediction of vertical fluxes of nutrients and other dissolved materials in Long Island Sound.

## 1. Introduction

Primary production in the ocean is controlled to a large extent by vertical nutrient fluxes from the nutrient-rich deep water into the overlying euphotic zone. While direct measurements of these fluxes are generally lacking due to experimental difficulties, considerable effort has been made to study vertical nutrient transport using theoretical models. In early studies (e.g. Jamart *et al.*, 1977; Eppley *et al.*, 1979; Wroblewski and O'Brien, 1981), nutrient fluxes were estimated using a constant profile of the turbulent diffusion coefficient. More recently, Garside (1985) used a one-dimensional diffusion model together with high resolution measurements of nitrate concentrations to estimate nitrate fluxes in warm-core rings, and Lewis *et al.* (1986) estimated the supply of nitrate to the surface layer in an oligotrophic ocean from rates of turbulent kinetic energy dissipation. McGowan and Hayward (1978) inferred mixing of nutrients into the euphotic zone in the central gyre of the North Pacific from the observed increases in primary production and standing stock of zooplankton. These

1. Marine Sciences Research Center, State University of New York, Stony Brook, New York, 11794, U.S.A.

studies revealed the important contribution of nutrient fluxes to fuel "new" production. Recognizing the transient (as short as several hours) nature of the physical processes driving the nutrient entrainment, Klein and Coste (1984) used a turbulence closure model (Mellor and Yamada, 1974) to study effects of wind forcing on nutrient transport into the surface mixed layer in the open ocean. They found that the interaction between the wind stress and the wind-generated inertial current induced a pulsating character of nutrient fluxes, which can influence the temporal pattern of primary productivity.

Large fluctuations of turbulent entrainment, due both to wind stress and tidal mixing, can occur in shallow coastal waters. Therefore it is necessary to use a realistic mixing model to estimate nutrient fluxes into the mixed layer in estuaries and shallow seas. In this study, we examined vertical nutrient mixing in late summer in Long Island Sound. The simulation used a one-dimensional numerical model based on Mellor and Yamada's (1974) level 2 turbulence closure scheme. Our work differs from that of Klein and Coste (1984) in three important aspects. First, because the tidal mixing plays an important role in estuaries, there were two mixed layers instead of a single upper mixed layer. The nutrient entrainments through the pycnocline were driven by current shear instabilities at the base of the upper mixed layer and at the top of the lower mixed layer. Therefore, both wind forcing and tidal forcing were taken into account in the present study. Second, our study used observed atmospheric forcing data; the surface heat flux and the wind stress were calculated from observed air temperature and wind velocity. Finally, we allowed nutrient production and consumption in the water column; in contrast, Klein and Coste (1984) treated nutrients as conservative quantities.

## 2. Nutrient cycles in Long Island Sound

The seasonal patterns of nutrient cycling and primary production in Long Island Sound were described by Riley and coworkers (Riley, 1941; Harris, 1959). The Sound shows high levels of dissolved nutrients during the winter months when chlorophyll levels are low and temperature is at its yearly minimum. The two annual phytoplankton blooms, characteristic of temperate regions (Cushing, 1959), are reflected as peaks of chlorophyll in the spring and in the fall. The data reported here and used in the formulation of the model were from samples taken at approximately weekly intervals from a station in central Long Island Sound (Fig. 1). Nitrogenous nutrient concentrations (ammonium, nitrite, and nitrate) were measured by standard methods (Strickland and Parsons, 1972) and hydrographic data (temperature, salinity, conductivity) were measured using a Beckman induction salinometer.

In early spring, the phytoplankton bloom was triggered by rapid stratification of the water column, and was accompanied by a decrease in surface water nutrient concentrations (Fig. 2). The sound remained thermally stratified throughout the summer (Peterson, 1986; see also Fig. 2), and nutrient levels in surface waters

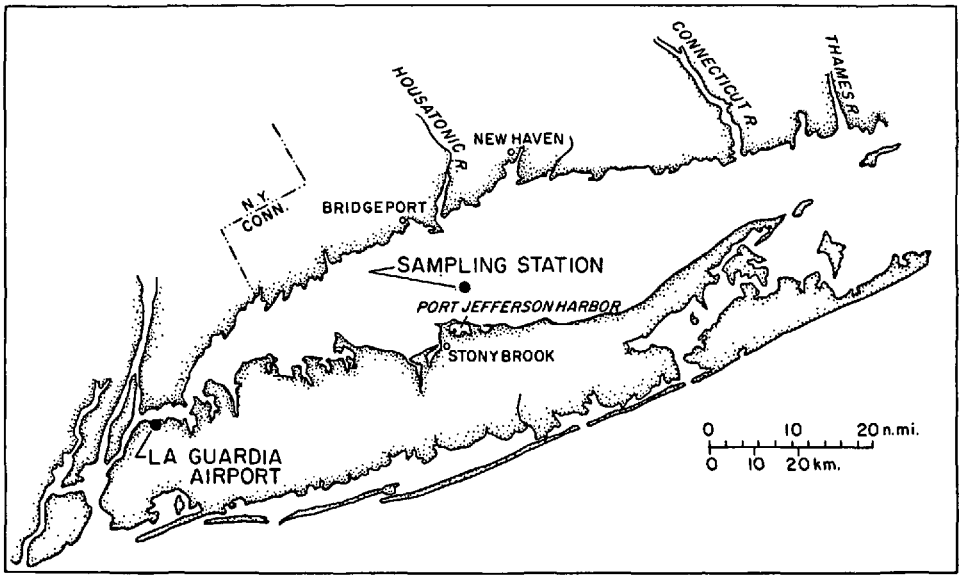


Figure 1. Map of the study region showing the sampling station and the weather station.

remained low (<1 $\mu$M). Nitrate concentrations were low throughout the water column (Riley and Conover, 1956; see also Fig. 2); the deep-water reservoir of ~5 $\mu$M nitrogen existed as ammonium (Fig. 2; Riley and Conover (1956) did not report ammonium concentrations). At the time of destratification of the water column in late August, there was a transient nitrite peak, after which the concentration of nitrate in the deep water increased, followed by the fall bloom of phytoplankton (Fig. 2).

The source of nitrate in the deep water during the late summer was probably bacterially-mediated ammonium oxidation. Advective transport of nitrate may not be important, because both residual currents and horizontal nitrate gradients were very weak during the late summer in central Long Island Sound (unpublished data). The mass balance among the various pools of dissolved inorganic nitrogen supports the hypothesis that ammonium oxidation was responsible for the increase in nitrate. Specifically, there was a ~5 $\mu$M decrease in ammonium concentrations, at the same time as the ~5 $\mu$M increase in nitrite concentrations. This was followed by a decrease in nitrite with a concomitant increase in nitrate (Fig. 2). The natural abundance of heavy nitrogen ($\delta^{15}N$) in the ammonium and nitrite + nitrate pools and incubation experiments with added $^{15}N$ (Horrigan *et al.*, 1986) confirm that the bacterial process of nitrification occurred at this time. Why the nitrification did not occur earlier in the summer is not clear, since the substrate (ammonium) was present in the deep water from early summer (Fig. 2). Two possibilities are: (1) the process is limited by low temperatures such that nitrification can occur only when the deep waters warm sufficiently, and (2) the process is limited by the number of organisms (catalytic sites)

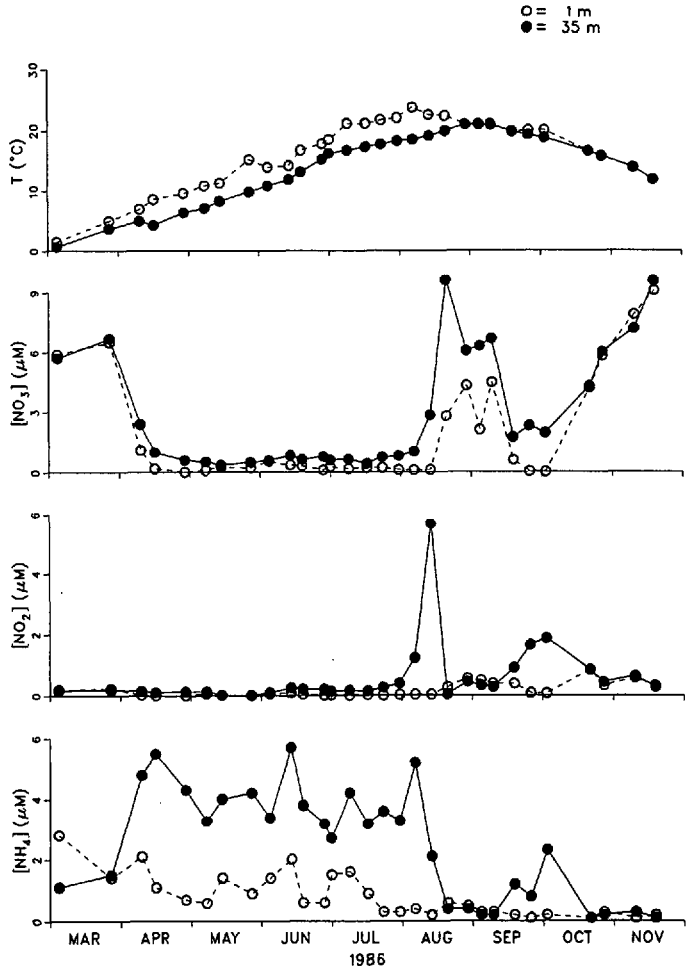


Figure 2. Observed time series of (a) water temperature; (b) nitrate; (c) nitrite; and (d) ammonium.

such that nitrification can occur only after a sufficient population of nitrifying bacteria has accumulated.

Phytoplankton uptake of ammonium and nitrate occurs in surface waters where light is available for phytoplankton growth. The ammonium pool was generally small (Fig. 2) and turns over rapidly (Table 1). Nitrate uptake was lower than ammonium, and remineralization of nitrate was not measurable in surface waters until September (Table 1). For most of the summer, then, the source of nitrate to the surface waters must be a nitrate flux across the thermocline. We assumed that this nitrate flux is taken up by phytoplankton in the euphotic zone.

Nitrate was chosen as the representative nutrient in the formulation of the model for several reasons: (1) rapid recycling of nitrate in the euphotic zone does not occur, (2)

Table 1. Rates of uptake and remineralization in surface waters from incubation experiments using added $^{15}N$ labelled substrates.

| | $NH_4^+$ | | | $NO_3^-$ | | |
|---|---|---|---|---|---|---|
| Month | Uptake | RPI* | Remineralization** | Uptake | RPI* | Remineralization** |
| Mar | 0.059 | 4.90 | 0.448 | 0.009 | 0.16 | — |
| Jun | 0.154 | 1.10 | 0.892 | 0.012 | 0.46 | — |
| Jul | 0.129 | 1.03 | 0.756 | 0.012 | 0.75 | — |
| Aug | 0.118 | 1.45 | 0.207 | 0.023 | 0.39 | — |
| Sep | 0.163 | 1.70 | 0.669 | 0.009 | 0.12 | 0.104 |

*RPI = relative preference index: % of total uptake/% of total pool size (McCarthy *et al.*, 1977).

**Calculated according to Garside and Glibert (1984).

Note: Uptake and remineralization are in μmole/l/hour. A dash indicates undetectable rates.

the source of nitrate (nitrification in the deep layer) has been demonstrated and therefore can be modeled, (3) the sink for nitrate (phytoplankton uptake in the euphotic zone) can be demonstrated and modeled during much of the summer season. The time period over which the model was run is the summer season, from 23 July to 29 August 1986. During this period, reasonable assumptions concerning the sources and sinks of nitrate can be made. In addition, this time period includes the erosion of the pycnocline and the event of destratification.

Historical patterns of oxygen concentrations show occasional surface supersaturation during the spring and summer, and declining levels of oxygen in the bottom water during the spring and summer (Riley and Conover, 1956). Oxygen supersaturation in surface waters is due to photosynthetic activity, whereas consumption of oxygen in the deep water is probably due to the decomposition of organic matter. For the complete oxidation of each mole of organic matter, 138 moles of oxygen are consumed (Redfield *et al.*, 1963). From the stoichiometry of the decomposition equation, 32 moles of oxygen (23% of the total) are required for the oxidation of ammonium to nitrate. Although we had no measurement of the concentrations, sources, and sinks of oxygen during the time period over which the model was run, we included oxygen as a dependent variable because the downward oxygen transport is important in controlling water quality.

## 3. Model formulation

*a. Basic equations.* The governing equations are

$$\frac{\partial u}{\partial t} - fv = -\frac{1}{\rho}\frac{\partial p}{\partial x} + \frac{\partial}{\partial z}\left(-\overline{w'u'} + \nu\frac{\partial u}{\partial z}\right) - Du \tag{1a}$$

$$\frac{\partial v}{\partial t} + fu = -\frac{1}{\rho}\frac{\partial p}{\partial y} + \frac{\partial}{\partial z}\left(-\overline{w'v'} + \nu\frac{\partial v}{\partial z}\right) - Dv \tag{1b}$$

$$\frac{\partial T}{\partial t} = \frac{\partial}{\partial z}\left(-\overline{w'T'} + \nu\frac{\partial T}{\partial z}\right) \tag{2}$$

$$\frac{\partial S}{\partial t} = \frac{\partial}{\partial z}\left(-\overline{w'S'} + \nu\frac{\partial S}{\partial z}\right) \tag{3}$$

$$\frac{\partial N}{\partial t} = \frac{\partial}{\partial z}\left(-\overline{w'N'} + \nu\frac{\partial N}{\partial z}\right) + \Psi \tag{4}$$

where $t$ is time, $x$, $y$ and $z$ the space coordinates, $u$ and $v$ the $x$-and $y$-components of the current velocity, $T$ the temperature, $S$ the salinity, $N$ the nitrate concentration, $p$ the pressure, $f$ the Coriolis parameter, $D$ a damping factor, $\nu$ a background diffusion coefficient, $\overline{w'u'}$ and $\overline{w'v'}$ the turbulent Reynolds stress, $\overline{w'T'}$, $\overline{w'S'}$ and $\overline{w'N'}$ the vertical eddy fluxes of heat, salt, and nitrate, respectively, and $\Psi$ the sink or source of the nitrate. The transport equation for the oxygen is the same as that for the nitrate (Eq. 4).

The horizontal pressure gradients in Eqs. (1a,b) were assumed to be caused by a barotropic tidal wave which acts as a periodic forcing. A drag force (the rightmost term in Eqs. (1a,b)) was introduced in the model to attenuate inertial oscillations. Without this damping force, the model predicted a suspiciously strong inertial current in the first several days of the simulation period. In this study, $D$ was taken to be $0.1f$, which is considered a realistic value (Clancy and Pollak, 1983). The terms involving $\nu$ in Eqs. (1)–(4) account for the background diffusion. We took $\nu = 0.5$ cm$^2$/s, which is a little larger than that used by Mellor and Durbin (1975). The larger diffusion value in the Sound may be related to the enhanced mixing in the shallow banks.

The vertical eddy fluxes of momentum, heat, salt and nutrient were parameterized according to the level 2 turbulence closure model of Mellor and Yamada (1974), i.e.

$$(\overline{w'u'}, \overline{w'v'}) = -\iota q S_M\left[\frac{\partial u}{\partial z}, \frac{\partial v}{\partial z}\right] \tag{5}$$

$$(\overline{w'T'}, \overline{w'S'}, \overline{w'N'}) = -\iota q S_H\left[\frac{\partial T}{\partial z}, \frac{\partial S}{\partial z}, \frac{\partial N}{\partial z}\right] \tag{6}$$

where $\iota$ is the mixing length, $q$ the square root of twice the turbulence kinetic energy, and $S_M$ and $S_H$ are functions of the gradient Richardson number

$$R_i = \frac{-\frac{g}{\rho}\frac{\partial \rho}{\partial z}}{\left(\frac{\partial u}{\partial z}\right)^2 + \left(\frac{\partial v}{\partial z}\right)^2} \tag{7}$$

where density $\rho$ is calculated from $T$ and $S$ according to the Knudson formula (Fofonoff, 1962). When $R_i$ exceeds a critical value (0.23), $S_M = S_H = 0$, and turbulent

mixing is suppressed by the density stratification. $q$ was determined from a simplified turbulence energy equation

$$\iota q S_M \left[\left(\frac{\partial u}{\partial z}\right)^2 + \left(\frac{\partial v}{\partial z}\right)^2\right] + \iota q S_H \left[\frac{g}{\rho}\frac{\partial \rho}{\partial z}\right] - \frac{q^3}{15\iota} = 0 \tag{8}$$

which represents a local balance between shear production, buoyancy production, and dissipation.

To complete the turbulence closure the mixing length scale $\iota$ must be specified. According to Blackadar (1962), $\iota$ can be defined as

$$\iota = \frac{\kappa\lambda}{1 + \kappa\lambda/\iota_0} \tag{9}$$

where $\kappa$ is the von Karman constant and $\lambda$ the distance from the boundary. Near the boundary $\iota \sim \lambda$, which yields a logarithmic velocity layer, while far from the boundary $\iota \sim \iota_0$. The asymptotic scale $\iota_0$ can be simply determined by the ratio of the first to the zeroth moment of $q$ in the mixed layer (e.g., Mellor and Durbin, 1975; Weatherly and Martin, 1978). In our case, two separate calculations of $\iota_0$ were made since turbulence has different sources and vertical extents in the two mixed layers. Letting $z = 0$ at the water surface, we have

$$\iota_0 = \begin{cases} \alpha \int_{-h_1}^{0} |z| q \, dz \Big/ \int_{-h_1}^{0} q \, dz, \text{ upper layer} \\ \alpha \int_{-H}^{h_2 - H} |H + z| q \, dz \Big/ \int_{-H}^{h_2 - H} q \, dz, \text{ lower layer} \end{cases} \tag{10}$$

where $\alpha$ is a constant, $H$ the water depth, and $h_1$ and $h_2$ the depth of the upper and the lower mixed layer, respectively. Following Weatherly and Martin (1978), we chose $\alpha = 0.3$. The mixed layer depth is the distance from the boundary where turbulence energy vanishes. When the two mixed layers merge, $h_1 = h_2 = H$. From Eqs. (9) and (10), the mixing length $\iota$ was determined.

*b. Initial conditions.* The initial profiles of temperature, salinity, and nitrate concentration were obtained from a linear interpolation of measurements at depths 1, 3, 5, 10, 15, 20, 30, and 38 m on July 23, 1986. Since no oxygen measurement was available, we assumed that the initial profile of oxygen concentration had the same shape as the temperature profile with a concentration of 230 μmole/l at surface and 200 μmole/l at bottom. The initial velocity fields were obtained by running the model for 10 tidal cycles starting from rest, driven by a constant wind stress equal to that at the starting time but with no surface heat flux. The initial phase of tidal current was estimated from the 1986 Tidal Current Tables.

*c. Boundary conditions.* The surface fluxes of momentum and heat were specified as

$$(\iota q S_M + \nu)\left(\frac{\partial u}{\partial z}, \frac{\partial v}{\partial z}\right) = (\tau_x, \tau_y) \qquad \text{at } z = 0 \tag{11}$$

$$(\iota q S_H + \nu)\frac{\partial T}{\partial z} = k(T_a - T_s) \tag{12}$$

where $\tau_x$ and $\tau_y$ are $x$-and $y$-components of wind stress (divided by water density), $k$ a heat exchange coefficient, and $T_a$ and $T_s$ the air and the water surface temperature, respectively. We took $k = 10^{-3}$, which is comparable to $k = 0.8 \times 10^{-3}$ suggested by Haney (1971). The wind stress was calculated from

$$\tau = \rho_a C_d |W| \mathbf{W} \tag{13}$$

where $\mathbf{W}$ is the wind velocity vector, $\rho_a$ a reference air density, and $C_d$ a drag coefficient determined according to Large and Pond (1981). The surface boundary conditions for salinity and nitrate were no flux. The boundary condition for oxygen was that the surface water is always saturated with oxygen (~230 $\mu$mol/l).

At the bottom, we assumed no flux of heat, salt, or nitrate. However, an oxygen flux of 30 mmole/m$^2$/day was included to account for benthic oxygen consumption (Mackin, pers. commun.). To satisfy the turbulence law of the wall, the near bottom velocity was set to

$$(u,v) = [(\overline{w'u'}, \overline{w'v'})/\kappa u_*] \ln[H + z)/z_0] \quad \text{as } z \rightarrow -H \tag{14}$$

where $u_*$ is the bottom friction velocity and $z_0$ the roughness height (0.1 cm in this study). The model was not sensitive to the choice of $z_0$ (Weatherly and Martin, 1978; Oey *et al.*, 1985).

*d. Method of computation.* The finite difference scheme follows Mellor and Durbin (1975). The resulting two-time-step, implicit finite difference equation was solved with a tri-diaganol matrix reduction technique. At each time step an iteration was performed to determine eddy diffusion coefficients. A vertical grid of 21 levels was used for a water column of 40 m depth. To have a fine resolution near surface and near bottom, the grid spacing adjacent to boundaries was set to 0.5 m. The grid spacing increases exponentially to 3 m in a distance of 8 m from the boundaries, and thereafter it is a constant 3 m interval. A time increment of 1 hour was used in order to resolve tidal variability.

*e. Model forcing.* The model was driven by atmospheric forcing through surface boundary conditions. Three-hourly records of wind velocity and air temperature from LaGuardia Airport (see Fig. 1) were linearly interpolated into hourly time series for model input. During the simulation period the wind stress was highly variable (Fig. 3a), and the air temperature had a decreasing trend superimposed by diurnal

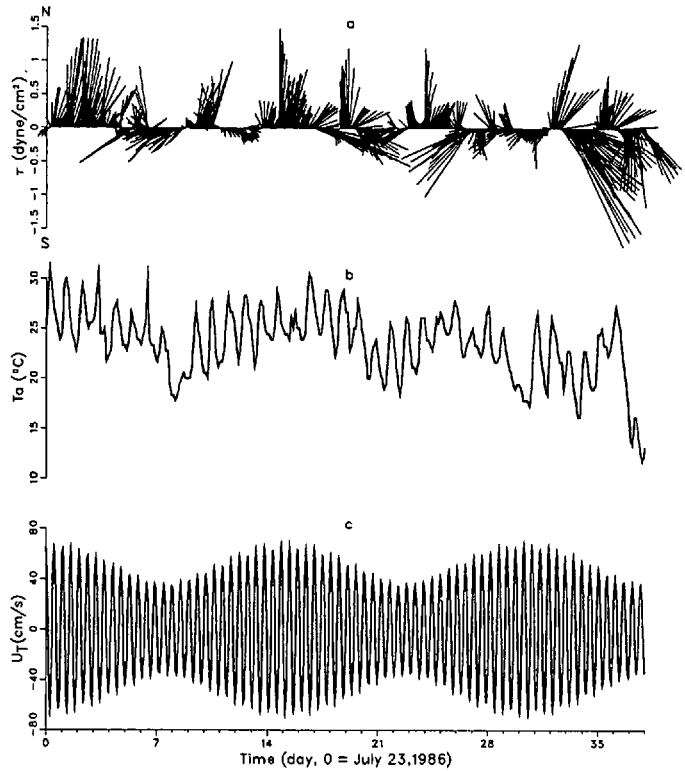


Figure 3. Time series of (a) wind stress; (b) air temperature; and (c) tidal current. Wind stress and air temperature are from records from LaGuardia Airport. Tidal current velocity is based on 1986 Tidal Current Table (see text).

fluctuations (Fig. 3b). The air temperature dropped after each northerly wind. This was most evident in late August when the air temperature decreased abruptly following a very strong northwesterly wind.

Tidal forcing was incorporated into the model through the pressure gradient terms in Eqs. (1a, b). We assumed that the horizontal pressure gradient is caused by a Kelvin tidal wave, i.e.

$$-\frac{1}{\rho}\left(\frac{\partial p}{\partial x}, \frac{\partial p}{\partial y}\right) = \left(\frac{\partial U_t}{\partial t}, f U_T\right) \tag{15}$$

where $U_t$ is the current velocity in the direction of wave propagation. Since the tidal current in Long Island Sound is semidiurnal, modulated by a fortnightly period, we let

$$U_T = U_m \cos(\omega_m t + \Phi_m) + U_s \cos(\omega_s t + \Phi_s) \tag{16}$$

where $U$ is the amplitude, $\omega$ the frequency, and $\Phi$ the phase; subscripts $m$ and $s$ denote $M_2$ and $S_2$ tides, respectively. Based on 1986 Tidal Current Table, we chose $U_m$ = 50 cm/s, $U_s$ = 20 cm/s, and $\Phi_m = \Phi_s = 0$ (Fig. 3c).

A time- and depth-dependent source term ($\Psi$ in Eq. (4)) for the nitrate was assigned

$$\Psi(z, t) = \begin{cases} -\gamma N, & 0 \geq z \geq -5 \text{ m} \\ \beta(t) N, & \text{else} \end{cases} \tag{17}$$

where

$$\gamma = 0.04 \text{ hr}^{-1}, \beta(t) = \begin{cases} 0.008 \text{ hr}^{-1}, \text{ 13th day} \leq t \leq \text{29th day} \\ 0, \text{ else} \end{cases}$$

The nitrate sink in the upper 5 m reflects phytoplankton uptake. The nitrate source below the euphotic zone for the period from August 5 to 21 (day 13 to 29) was due to bacterially-mediated nitrification. Before August 5, ammonium oxidation did not appear to occur, and after August 21, the substrate (ammonium) was depleted and the nitrate production ceased. Eq. (17) implies an exponential increase in nitrate concentration, which is consistent with the exponential growth rate of both phytoplankton and nitrifying bacteria.

The $\Psi$ for oxygen was stoichiometrically calculated from that for nitrate, since the surface sink and the deep source for nitrate correspond to a surface source and a deep sink for oxygen. In essence, for each N oxidized, 2 $O_2$ are used:

$$NH_4^+ + 2O_2 \rightarrow NO_3^- + H_2O + 2H^+ \tag{18}$$

An additional sink for oxygen is the oxidation of organic carbon, which was not included in the model due to our lack of data on this process. The reservoir of ammonium below the pycnocline over much of the summer (see Fig. 2d) indicated that the oxidation of organic carbon and ammonium were not closely coupled. Assumptions concerning the consumption of oxygen due to carbon oxidation are thus unwarranted. The model results, then, present a high limit of oxygen concentrations, considering only ammonium oxidation as an oxygen sink in the deep layer.

## 4. Results

The model was integrated over the period from July 23 to August 29, 1986. The vertical profiles of the computed temperature and nitrate concentration were compared with the measurements available in that period (Fig. 4). The agreement between the model results and the measured data generally was very good. Figure 5 shows the model-computed vertical structures of temperature, salinity, nitrate and oxygen for the study period. Temperature generally was uniform in a surface layer of 5 m and in a

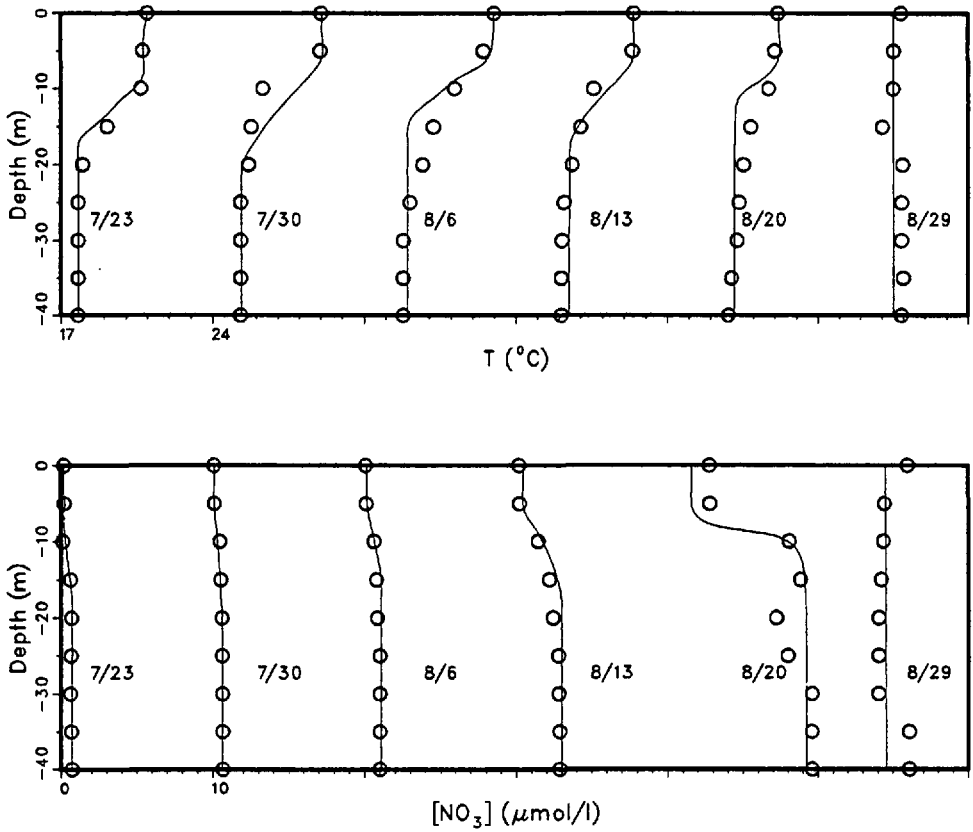


Figure 4. Proflies at different times of (a) water temperature and (b) nitrate. Circles represents measurements and solid lines are computations.

bottom layer of 20 ~ 25 m, with a strong thermocline in between (Fig. 5a). The temperature in the bottom mixed layer increased gradually due to a downward heat flux through the thermocline. Entrainment of warm water from above the thermocline was caused by the tidal stirring in the lower layer. The temperature in the surface mixed layer had diurnal variations (generally less than 0.5°C) in response to the diurnal heating, and longer period (about 10 days) fluctuations in response to the atmospheric forcing. Spring-neap tide and surface warming-cooling caused the thermocline to squeeze (e.g. around day 16) and to stretch (e.g. around day 23), but the thermocline persisted until day 33 (August 24) when the combined effects of surface cooling, strong wind, and spring tidal current completely broke down the stratification. Afterwards, the main thermocline never recovered, although small surface temperature fluctuations still occurred.

The halocline was rapidly eroded by turbulent mixing (Fig. 5b). In this model, the salt content in the water column was conserved because there was no salt flux through

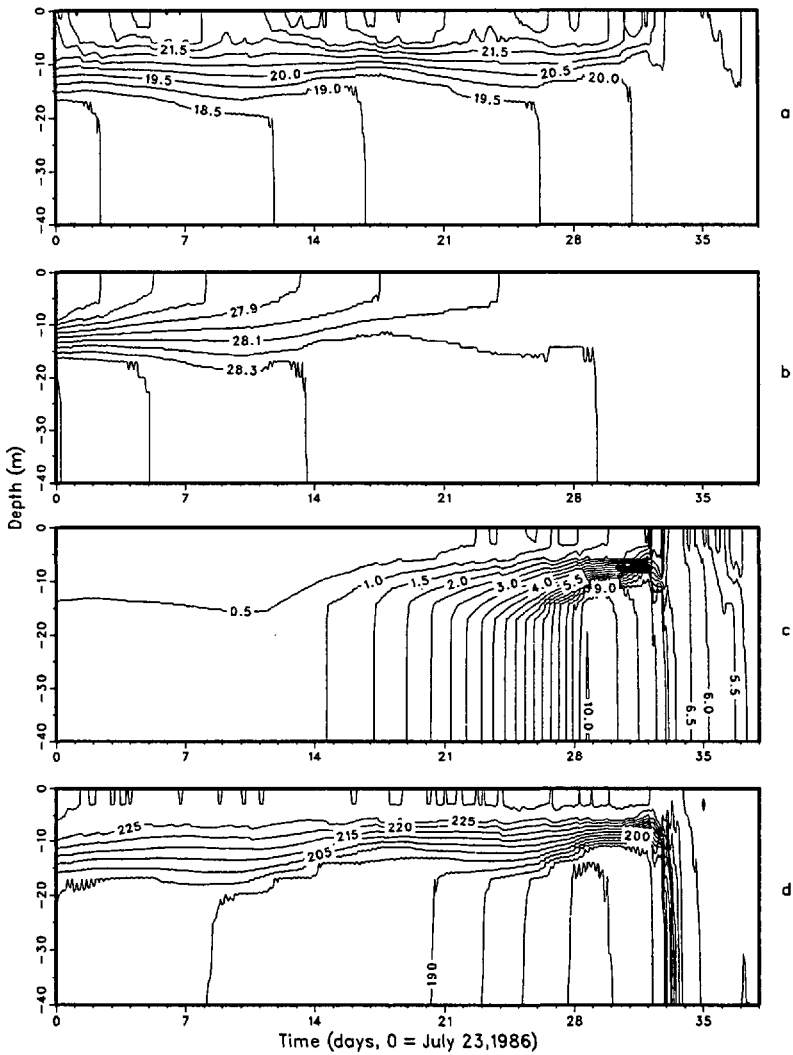


Figure 5. Model-predicted time-depth contours of (a) temperature (°C); (b) salinity (‰); (c) nitrate ($\mu$mole/l); and (d) oxygen ($\mu$mole/l).

the boundaries. The result suggested that, even when the water column was stratified, turbulent mixing was strong enough to mix a conservative property completely from a stratified initial state in about 20 days. This rapid mixing was mainly caused by the wind- and tidally-induced turbulent diffusion, and not by the background diffusion. On the other hand, the observed salinity profiles indicated that a weak halocline persisted through day 33. The observed halocline was probably maintained by an estuarine circulation which resulted in a salinity increase in the lower layer and a salinity decrease in the upper layer.

The nitrate distribution (Fig. 5c) was controlled by the sink in the surface layer, the source in the lower layer, and the flux through the nutricline. During the first 12 days, there was no nitrate source, and a slight decrease of the nitrate concentration in the surface layer indicated that the upward nitrate flux was less than the rate of phytoplankton uptake in the surface layer. After day 12, nitrate was produced in the lower layer. The increase of the nitrate concentration through the whole water column indicated that the nitrate flux through the nutricline was less than the gain in the lower layer, but was greater than the loss in the upper layer. On day 29, the nitrate source ceased, so the nitrate concentration in the lower layer began to decrease again. Four days later, when density stratification broke down, the nitrate was mixed up through the water column. It is worth noting that there was a short recovery of nitrate stratification around day 36 in response to a brief surface warming. This indicates that, with the influence of phytoplankton uptake in the euphotic zone, the vertical nitrate structure is very sensitive to the density stratification.

The oxygen distribution (Fig. 5d) was similar to the temperature distribution. There were two well-mixed layers separated by a high gradient intermediate layer before day 33. The surface layer was always saturated with oxygen, although small oxygen fluctuations occurred due to variable wind mixing. The oxygen concentration in the lower layer decreased slowly during the first 12 days, indicating the downward oxygen flux through the thermocline was slightly less than the benthic oxygen loss. On day 12, the oxygen consumption started to accelerate due to the nitrification in the water column. However, because of increased downward oxygen flux associated with a spring tide, rapid decrease of the oxygen concentration in the lower layer occurred several days later. After day 29, the oxygen concentration began to increase because the nitrification had stopped and the downward oxygen flux through the thermocline exceeded the oxygen loss at the bottom. On day 33 when the destratification occurred, the whole water column became oxygen saturated.

Figures 6a and 6b show the time history of the net flux of nitrate into the upper mixed layer ($FN$) and the net flux of oxygen into the lower mixed layer ($FO$). They are determined from

$$FN = \frac{d}{dt}\int_{-5\text{m}}^{0} [NO_3]\, dz, \quad FO = \frac{d}{dt}\int_{-40\text{m}}^{-25\text{m}} [O_2]\, dz \tag{19}$$

The maximum fluxes of both nitrate and oxygen occurred around day 33. The mean nitrate flux was low during the first 12 days because of the stable stratification and the low level of nitrate in the lower layer. The flux increased exponentially as the concentration of nitrate in the lower layer increased. An interesting feature of the upward nitrate transport was the large pulses of about one day duration with amplitudes much larger than the mean flux (note the logarithmic scale used in Fig. 6a,b). This highly unsteady nitrate supply could cause large variabilities in phytoplankton production. Klein and Coste (1984) suggested that the pulsating

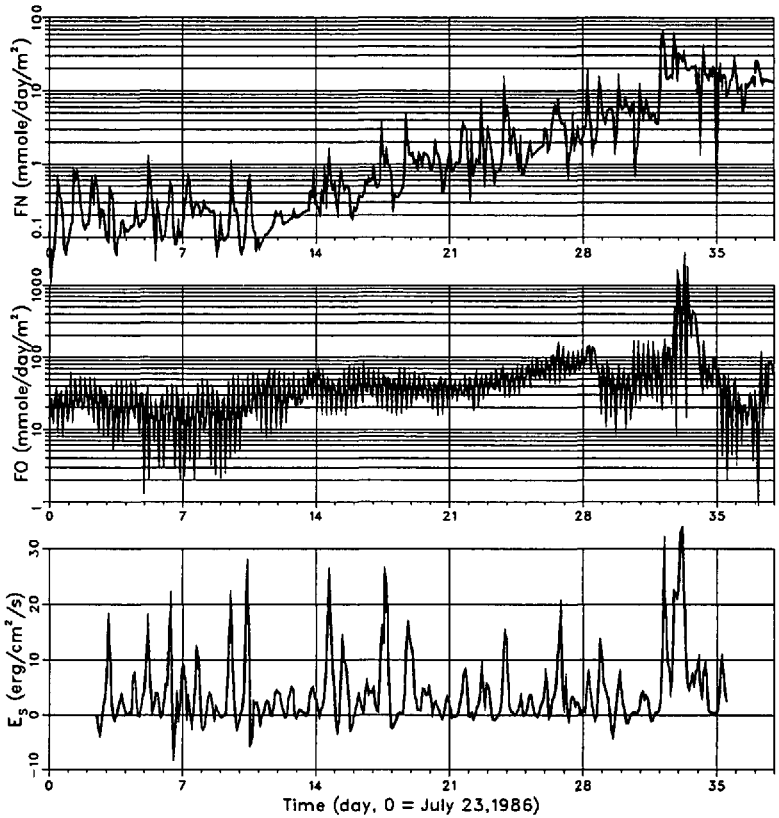


Figure 6. Model-predicted time series of (a) nitrate flux into the upper mixed layer; (b) oxygen flux into the lower mixed layer; and (c) surface energy input by wind.

nutrient entrainment into the upper mixed layer is induced by the interaction between wind stress and wind-induced surface current. In our case, the surface currents included inertial currents as well as tidal currents. Consequently, we estimated the wind energy influx by computing the product of the wind stress and the tidally averaged surface current (Fig. 6c). The large pulses of the nitrate flux into the upper layer clearly were correlated with the peaks of the surface energy flux. In other words, entrainments through the upper thermocline were indeed driven by the wind-supplied energy. The downward oxygen flux into the lower mixed layer was characterized by fluctuations of a semi-tidal (~6 h) period and of a fortnightly period of tidal origin. The mean oxygen flux was larger when nitrification was active because of the larger vertical gradient of oxygen during that period.

Figure 7 shows the vertical structures of the mean velocity shear ($U_z = ((\partial u/\partial z)^2 + (\partial v/\partial z)^2)^{1/2}$), the squared buoyancy frequency ($N^2 = -1/\rho(\partial\rho/\partial z)$), and the tidally averaged eddy diffusivity ($A_H = q\iota S_H + \nu$). The mean velocity shears (Fig. 7a) had high values at the bottom of the upper mixed layer and at the top of the lower mixed

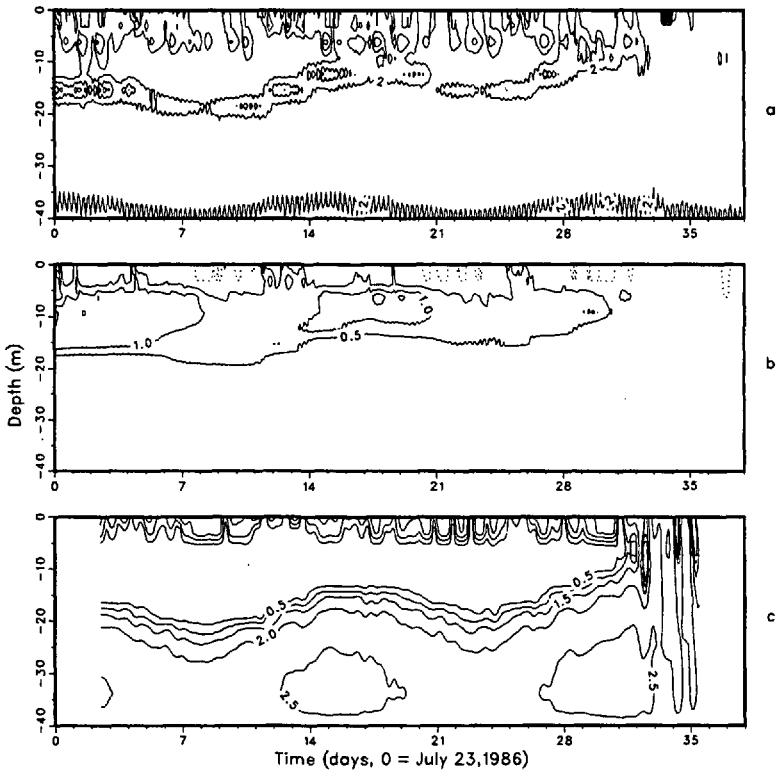


Figure 7. Model-predicted time-depth contours of (a) means velocity shear ($U_z \times 10^2$); (b) squared buoyancy frequency ($N^2 \times 10^3$); and (c) tidally averaged vertical eddy diffusivity ($\log_{10}(A_H)$).

layer. The turbulence produced by strong shear instabilities periodically eroded the thermocline. Mean velocity shears in the upper layer were characterized by quasi-inertial fluctuations, while those in the lower layer were characterized by tidal fluctuations. The buoyancy frequency (Fig. 7b) was high in the thermocline and decreased rapidly toward the mixed layers. However, when strong surface heating was coupled with weak wind stress (for example, around day 12), the density gradient could develop rapidly in the surface layer. The eddy diffusivity had strong fluctuations of 6-hour period in the lower mixed layer; the amplitudes were larger than 100 $cm^2/s$ during spring tides. However, for clarity, only tidally averaged values are shown in Fig. 7c. The eddy diffusivity in the mixed layers was 2 ~ 3 orders of magnitude larger than the background diffusivity, and its values generally were much higher in the lower layer than in the upper layer.

## 5. Discussion

A simple one-dimensional mixed-layer model has successfully predicted the evolution of the vertical structures of temperature and nitrate in the late summer in central

Long Island Sound. We found that the destratification at the end of the summer took place under the favorable combination of strong wind, strong surface cooling, and spring tide. During the simulation period, this combination occurred only around day 33 (August 24), although one factor or a combination of two had happened in several occasions before. For example, around day 15, a spring tide and a very strong wind were present, but there was no surface cooling. The thickness of the lower mixed layer increased, but the surface mixed layer remained unchanged, and consequently the thermocline was squeezed instead of being destroyed. What happened in the event of destratification was a rapid thickening of both mixed layers, followed by a sudden breakup of the thermocline and eventually a complete mixing of the water column. The relieved vertical fluxes of nutrients were an order of magnitude higher than the normal flux, which probably led to the fall phytoplankton bloom.

There is always a non-negligible vertical nutrient transport even under weak wind. Consequently, the phytoplankton uptake of nutrients in the surface layer must be taken into account in modeling the nutricline. The nutrient flux into the surface layer is highly correlated with the surface energy flux of wind stress. The pulsating character of this flux is consistent with that found in Klein and Coste (1984). The nutrient transport through the thermocline is driven by the erosion of the thermocline from both sides. The tidally-induced turbulence at the base of the thermocline injects nutrients into the thermocline, while the wind induced turbulence at the top of the thermocline entrains nutrients into the upper layer. The thermocline (nutricline) serves as a reservoir for nutrients.

An issue of biological significance is the nitrification modeled in this study. Either the activity of nitrifying bacteria is greatly enhanced when the temperature in the lower layer increases to a certain degree, or the population of nitrifying bacteria is so small before mid-summer that they have little impact on nitrate concentration. The nitrification results in a much higher nitrate concentration in the lower layer, leading to a strong nutricline (for nitrate) and a larger upward nitrate flux. As far as total dissolved inorganic N is concerned, it does not matter if there is nitrification or not, since the total N transported into the surface layer will be the same. However, the nitrification could cause a compositional transition in phytoplankton population as the upward flux of nitrate dominates that of ammonium. Incubation experiments using added $^{15}N$-labelled substrates confirmed that nitrate uptake by phytoplankton is greater in the late summer (August) than at other times of the year (Table 1). Although recycling of ammonium in the surface layer remains the dominant source of nitrogen to the phytoplankton community, the relatively greater importance of nitrate in August may lead to the fall bloom of phytoplankton. The fall bloom of phytoplankton is dominated by diatoms, as opposed to the dinoflagellates which dominate during the summer stratified season (Peterson, 1986).

The oxygen flux into the lower layer is controlled by the tidal mixing. The thermocline again serves as a reservoir for oxygen. The wind-induced turbulence at the

top of the thermocline transports oxygen into the thermocline, while the tidally-induced turbulence at the base of the thermocline entrains the oxygen into the lower layer. In our case, the oxygen flux through the thermocline, the oxygen consumption in the water column due to nitrification, and the oxygen loss at the bottom have comparable magnitudes during the period of stratification. However, due to lack of measurements, we are unable to verify that result.

*Acknowledgments.* This project is partially supported by the Institute for Naval Oceanography, and by NSF grants OCE-8417595, OCE-8743222, and OCE-8214932. Support from NY State Sea Grant to W.T. Peterson enabled the collection of field samples. We thank J. Mackin for critically reviewing the manuscript and J.J. McCarthy for access to mass spectrometric facilities. This is MSRC contribution number 615.

## REFERENCES

Blackadar, A. K. 1962. The vertical distribution of wind and turbulent exchange in a neutral atmosphere. J. Geophys. Res., *67,* 3095–3102.

Clancy, R. M. and K. D. Pollak. 1983. A real-time synoptic ocean thermal analysis/forecast system. Prog. Oceanogr., *12,* 383–424.

Cushing, D. H. 1959. The seasonal variation in oceanic production as a problem in population dynamics. J. Cons. Perm. Int. Explor. Mer, *24,* 455–464.

Eppley, R. W., E. H. Renger and W. G. Harrison. 1979. Nitrate and phytoplankton production in southern California coastal waters. Limnol. Oceanogr., *24,* 483–494.

Fofonoff, N. P. 1962. Physical properties of sea-water, *in* The Sea, Vol. 1, Wiley-Interscience, 3–30.

Garside, C. 1985. The vertical distribution of nitrate in open ocean surface water. Deep-Sea Res., *32,* 723–732.

Garside, C. and P. M. Glibert. 1984. Computer modeling of $^{15}N$ uptake and remineralization experiments. Limnol. Oceanogr., *29,* 199–204.

Haney, R. L. 1971. Surface thermal boundary condition for ocean circulation models. J Phys. Oceanogr., *1,* 241–248.

Harris, E. 1959. The nitrogen cycle in Long Island Sound. Bull. Bingham Oceanogr. Coll., *17,* 31–65.

Horrigan, S. G., J. P. Montoya, J. J. McCarthy and W. T. Peterson. 1986. $^{15}N$ isotopic discrimination during nitrification at different substrate concentrations. EOS, *67,* 988–989.

Jamart, B. M., D. F. Winter, K. Banse, G. C. Anderson and R. K. Lam. 1977. A theoretical study of phytoplankton growth and nutrient distribution in the Pacific Ocean off the northwestern U.S. coast. Deep-Sea Res., *24,* 753–773.

Klein, P. and B. Coste. 1984. Effects of wind-stress variability on nutrient transport into the mixed layer. Deep-Sea Res., *31,* 21–37.

Large, W. G. and S. Pond. 1981. Open ocean momentum flux measurements in moderate to strong winds. J. Phys. Oceanogr., *11,* 324–336.

Lewis, M. R., W. G. Harrison, N. S. Oakey, D. Herbert and T. Platt. 1986. Vertical nitrate fluxes in the oligotrophic ocean. Science, *234,* 870–873.

McCarthy, J. J., W. R. Taylor and J. L. Taft. 1977. Nitrogenous nutrition of the plankton in the Chesapeake Bay. I. Nutrient availability and phytoplankton preferences. Limnol. Oceanogr., *22,* 996–1011.

McGowan, J. A. and T. L. Hayward. 1978. Mixing and oceanic productivity. Deep-Sea Res., *25,* 771–793.

Mellor, G. L. and P. A. Durbin. 1975. The structure and dynamics of the ocean surface mixed layer. J Phys. Oceanogr., *5,* 718–728.

Mellor, G. L. and T. Yamada. 1974. A hierarchy of turbulence closure models for planetary boundary layers. J. Atm. Sci., *31,* 1791–1806.

Oey, L.-Y., G. L. Mellor and R. I. Hires. 1985. A three-dimensional simulation of the Hudson-Raritan estuary. I: Description of the model and model simulation. J. Phys. Oceanogr., *15,* 1676–1692.

Peterson, W. T. 1986. The effects of seasonal variations in stratification on plankton dynamics in Long Island Sound, *in* Lecture Notes on Coastal and Estuarine Studies, *17,* M.J. Bowman, C. M. Yentsch and W. T. Peterson, eds., Springer-Verlag, Berlin, 297–320.

Redfield, A. C., B. H. Ketchum and F. A. Richards. 1963. The influence of organisms on the composition of sea-water, *in* The Sea, *2,* M.N. Hill, ed., Interscience, NY, 26–27.

Riley, G. A. 1941. Plankton studies. III. Long Island Sound. Bull. Bingham Oceanogr. Coll., *7,* 1–93.

Riley, G. A. and S. A. M. Conover. 1956. Oceanography of Long Island Sound, 1952–1954. III. Chemical oceanography. Bull. Bingham Oceanogr. Coll., *15,* 47–61.

Strickland, J. D. H. and T. R. Parsons. 1972. A practical handbook of seawater analysis, 2nd ed. Bull. Fish. Res. Board Canada, *167.*

Weatherly, G. L. and P. J. Martin. 1978. On the structure and dynamics of the oceanic bottom boundary layer. J. Phys. Oceanogr., *8,* 557–570.

Wroblewski, J. S. and J. J. O'Brien. 1981. On modelling the turbulent transport of passive biological variables in aquatic ecosystems. Ecological Modelling, *12,* 29–44.

Received: *23 February, 1988;* revised: *9 June, 1988.*